Available online at www.sciencedirect.com

ScienceDirect

Ceramics International 40 (2014) 4109–4116

CERAMICS INTERNATIONAL

www.elsevier.com/locate/ceramint

Graphene nanosheets-tungsten oxides composite for supercapacitor electrode

Yun Cai[a], Yan Wang[a], Shaojuan Deng[a], Gang Chen[a], Qing Li[a], Bingqian Han[a], Rong Han[a], Yude Wang[a,b,*]

[a]Department of Materials Science & Engineering, Yunnan University, 650091 Kunming, People's Republic of China
[b]State Key Lab of Silicon Materials, Zhejiang University, Hangzhou 310027, People's Republic of China

Received 29 July 2013; received in revised form 8 August 2013; accepted 14 August 2013
Available online 23 August 2013

Abstract

Graphene nanosheets-tungsten oxides (tungsten oxide/tungsten oxide hydrate mixture) (GNS-W) composite was successfully synthesized using a facile approach. $WO_3/WO_3 \cdot H_2O$ mixtures were deposited on the graphene nanosheets (GNS) to form the GNS-W composite. The GNS-W composite was characterized by X-ray diffraction (XRD), Raman spectrum, scanning electron microscopy (SEM), transmission electron microscopy (TEM) and X-ray photoelectron spectroscopy (XPS). The as-prepared GNS-W composite was directly fabricated into a supercapacitor electrode for potential energy storage application, and electrochemically tested by cyclic voltammetry, galvanostatic charge/discharge and electrochemical impedance spectroscopy. The GNS-W composite electrode exhibits a better electrochemical performance than that of the $WO_3/WO_3 \cdot H_2O$ mixtures electrode. A high specific capacitance of about 143.6 F g^{-1} at a current density of 0.1 A g^{-1} for the GNS-W composite delivers significant improvement than that for the $WO_3/WO_3 \cdot H_2O$ mixtures and GNS electrodes. The impedance studies also suggest that the GNS-W composite electrode shows the lower resistance and high conductivity due to the good interaction between the graphene nanosheets and the $WO_3/WO_3 \cdot H_2O$ mixtures. The good electrochemical performance for the GNS-W composite may be attributed to the interaction between the $WO_3/WO_3 \cdot H_2O$ mixtures and the edges of graphene nanosheets, which increases the ion diffusion rate as well as the conductivity.

Keywords: Graphene nanosheets; Tungsten oxides; Electrochemical capacitor; Pseudocapacitor; Electrochemical properties

1. Introduction

Supercapacitors have raised considerable attention over the past decades because of their higher power density and longer cycle life than secondary batteries and their higher energy density compared to conventional electrical double layer capacitors. As the ideal electrode materials of supercapacitors, RuO_2 and IrO_2 exhibit high specific capacitance value and high cycle capacity, which have been generated increasing interest in this field. However, their high cost and toxicity retard their wide application commercially. The development of alternative inexpensive and environmental friendly electrode materials with high performance has been one of the most active research fields of electrochemistry. Nowadays, many researchers develop various alternatives as a replacement for RuO_2 and IrO_2. Among the alternatives to RuO_2 and IrO_2, WO_3 may be one of the attractive candidates because of its environmental friendliness, low cost and electrochemical redox characteristics. It is well known that tungsten oxide (WO_3) is an important wide band gap n-type semiconductor and has many outstanding properties, such as electrochromic, optochromic, and gaschromic properties [1]. It has been extensively studied as a promising material for a multitude of potential applications including semiconductor gas sensors, electrode materials for secondary batteries, solar energy devices, photocatalysts, and field-emission devices [2–6]. The capacitive behaviors of tungsten oxides such as amorphous tungsten oxide, nanostructured tungsten trioxide, ordered mesoporous tungsten oxide, and so on, have been

*Corresponding author at: Yunnan University, Department of Materials Science and Engineering, Cuihu North Road 2, Kunming, Yunnan Province 650091, China. Fax: +86 871 5031410.
E-mail address: ydwang@ynu.edu.cn (Y. Wang).

0272-8842/$ - see front matter © 2013 Elsevier Ltd and Techna Group S.r.l. All rights reserved.
http://dx.doi.org/10.1016/j.ceramint.2013.08.065

investigated as supercapacitor electrode. [7–11]. $WO_3/WO_3 \cdot 0.5H_2O$ mixtures have been analyzed for pseudocapacitors by Chang et al [12]. However, the low electrical conductivity and poor rate performance of tungsten oxide pseudocapacitors have been their major demerits. To improve rate capability, resistance of supercapacitors should be minimized [11,13]. A new ordered mesoporous WO_{3-X} with a high electrical conductivity exhibited a high specific capacitance, a good rate capability and higher volumetric capacitance [7,11,14]. However, a great deal of attentions in capacitive behaviors has been focused on the preparations of tungsten oxide with various morphologies. On the other hand, most of the studies focused on WO_3 nanostructures which were made from mesoporous structures, nanorods or films. Research has seldom been focused on the capacitive properties based on the composite of WO_3 and carbon. If WO_3 is combined with highly conductive carbon or graphene sheets, its conductivity properties can be improved greatly [15], and will bring good capacitive materials with good conductivity of the system.

Graphene is a zero-gap semiconductor and considered as a promising material in various applications because of its unique electronic properties, excellent mechanical, optical, thermal and electrochemical properties, low-cost and environmentally benign nature. Nowadays, graphene has attracted great interest in the graphene composite materials, which comprise metal oxide nanoparticles, including ZnO [16], TiO_2 [17], SnO_2 [18], MnO_2 [19], CeO_2 [20], Co_3O_4 [21], and NiO [22]. These nanocomposites have good electrical conductivity and extra electrochemical properties, which could be potentially applicable in supercapacitors [16–23]. However, as promising electrode materials for supercapacitors, the investigation on graphene-metal oxide composite materials is not nearly enough so far. On the other hand, to the best of our knowledge, graphene nanosheets-tungsten oxide composite has been few researched as a supercapacitor electrode. To improve the electrical conductivity of tungsten oxides, many other methods have been carried out, such as template synthesis to ordered mesoporous WO_{3-X} and m-WO_{3-X}, microwave-assisted hydrothermal synthesis method to WO_3–$WO_3 \cdot 0.5H_2O$ mixtures [7,11,14], and so on. However, they required the template and a very stringent control in various processing parameters. Therefore, it is necessary to explore a new, facile and low-cost synthesis method for tungsten oxide to improve its electrical conductivity. In this work, we present graphene-tungsten oxide composite as electrode of supercapacitors. The graphene was fabricated by a modified Hummers method and glucose reduction process. The electrochemical measurements show that the GNS-W composite electrode enhances capacitive properties with better reversible charging/discharging ability and higher capacitance values than those of the tungsten oxide electrode.

2. Experimental

All the chemical reagents used in the experiments were obtained from commercial sources as guaranteed-grade reagents and used without further purification. Graphene oxide (GO) sheets were prepared from exfoliate graphite using a modified Hummers method [24,25]. GNS were prepared via using glucose as a reducing agent [26,27]. In a typical synthesis, exfoliation of GO was dispersed in water using an ultrasonic bath for 30 min to yield a homogeneous suspension. 1.2 g glucose was added to 40 mL of GO solution under stirring and then ammonia solution (25% w/w) was added into GO solution, followed by vigorous stirring. After vigorously shaking for a few minutes, the mixture was stirred for 60 min at 95 °C. The resulting black dispersion was then filtered and washed with water for several times and the obtained GNS was re-dispersed in water for further use.

To synthesize GNS-W, 40 mL of the as-obtained GNS suspension (0.5 mg L^{-1}) was transferred into a round bottom flask. 0.5 M HNO_3 is added to vigorously stirred solution of 10 mM $Na_2WO_4 \cdot 2H_2O$ dissolved in 10 mL of distilled water. The mixture solution was stirred for 30 min. Then the final mixture was added into the above GNS suspension. Finally, the resulting mixture was heated to 95 °C with stirring for 5 h. The mixture was centrifugally separated, and the precipitate was collected and dried at 100 °C for 24 h in a vacuum oven. The tungsten oxides were prepared as similar as above process without using GNS.

The electrochemical performances of as-obtained materials were investigated in an aqueous system (1 M H_2SO_4) using a three-electrode system. The working electrodes were fabricated by mixing the active materials, acetylene black and polytetrafluorene-ethylene (PTFE) binder at a weight ratio of 80:15:5. A small amount of alcohol was added to the mixture to produce a homogeneous paste, and pressed onto nickel foam current collectors to obtain electrodes. Platinum foil and Hg/HgO were used as the counter and reference electrodes, respectively. Cyclic voltammetry (CV) and electrochemical impedance spectra (EIS) measurements were conducted on a CHI660C electrochemical workstation (Shanghai Chenhua). The galvanostatic charge–discharge measurement was performed between 0 and 1.0 V (vs. Hg) on a LAND CT2001A Battery workstation at 25 °C (Wuhan Jinnuo Electronics, Ltd.).

Powder X-ray diffraction (XRD) characterization were carried out with a Rigaku TTRIII diffractometer with CuK_α radiation (λ=1.5406 Å). The samples were characterized by XRD at a rate of 0.1° min^{-1} in the 2θ range of 10°–90°. Scanning electron microscopy (SEM) analysis was performed by means of FEI QUANTA200 with microscope operating at 15 kV. The samples for SEM were prepared by dispersing the final powders in the conductive glue; this dispersing was then sprayed with gold. Transmission electron microscopy (TEM) measurement was performed on a Zeiss EM 912 Ω instrument at an acceleration voltage of 120 kV. The samples were prepared by spreading an ultrasonicated suspension in ethanol onto a grid and evaporating the solvent. X-ray photoelectron spectroscopy (XPS) was carried out at room temperature in ESCALAB 250 system. During XPS analysis, an Al Kα X-ray beam was adopted as the excitation source and the vacuum pressure of the instrument chamber was 1×10^{-7} Pa as read on the panel. Measured spectra were decomposed into Gaussian components by a least-square fitting method. Bonding

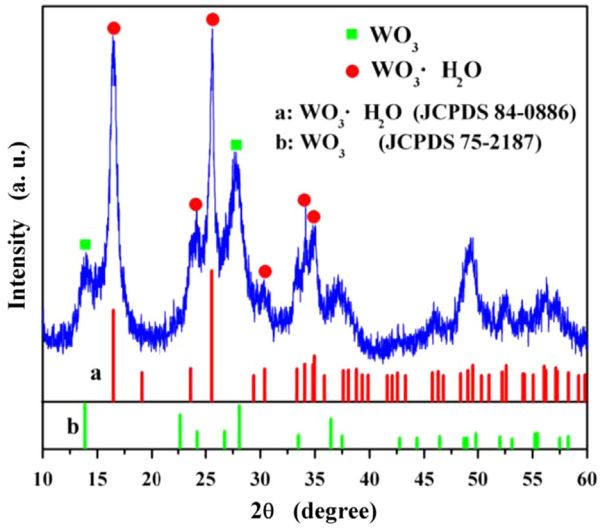

Fig. 1. XRD pattern of the GNS-W composite.

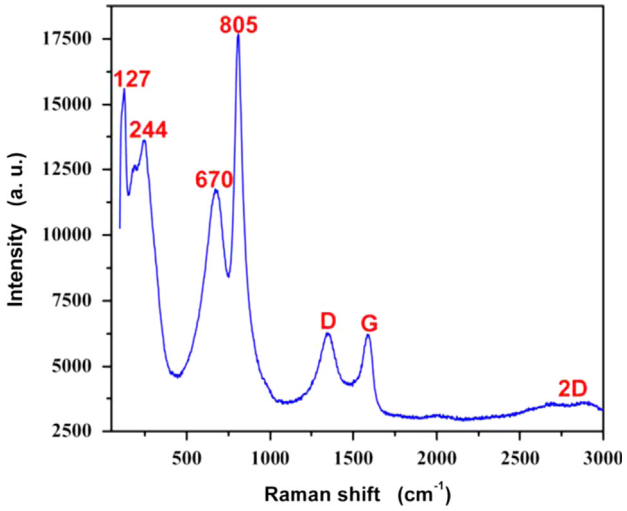

Fig. 2. Raman spectrum of the GNS-W composite.

energy was calibrated with reference to C1s peak (285.0 eV). The Raman spectrum was recorded with a Renishaw inVia Raman microscope, equipped with a CCD (charge coupled device) with the detector cooled to about 153 K using liquid N_2. The laser power was set at 30 mW.

3. Results and discussion

The powder X-ray diffraction pattern reveals the formation of the GNS-W composite, as shown in Fig. 1. The XRD pattern shows the presence of two crystalline phases, WO_3 (ICDD PDF No. 75-2187) and $WO_3 \cdot H_2O$ (ICDD PDF No. 84-0886). The results indicate that a mixture consisting of WO_3 and $WO_3 \cdot H_2O$ crystallites have been obtained. As shown in Fig. 1, the diffraction peak at about 26° for graphene is undistinguishable, indicating that significant face-to-face stacking is absent due to the introduction of WO_3 on both sides of graphene sheets [18].

For the crystalline WO_3, three main Raman spectral regions can be observed. One is between 900 and 600 cm^{-1}, the second one is between 400 and 200 cm^{-1}, and the third one is below 200 cm^{-1} [28]. The Raman spectrum of GNS-W composite is shown in Fig. 2. The characteristic peaks of tungsten oxide material appear in the region of 100–1000 cm^{-1}. The high-wavenumber region 805 and 670 cm^{-1} peaks are typical Raman peaks of the crystalline WO_3 [28], which correspond to the stretching and bending vibrations of the bridging tungsten and oxygen atoms. They are assigned to the W–O stretching (υ), and O–W–O deformation (γ) modes, respectively. The peak at 244 cm^{-1} is assigned to be the bending δ(O–W–O) vibrations. Those below 200 cm^{-1} modes were attributed to the lattice vibrations. All these peaks are in good accordance with those of other reports of tungsten oxides [28–31]. Raman spectroscopy is also an effective tool to study composites containing carbon phases and in particular graphene based structures with usual

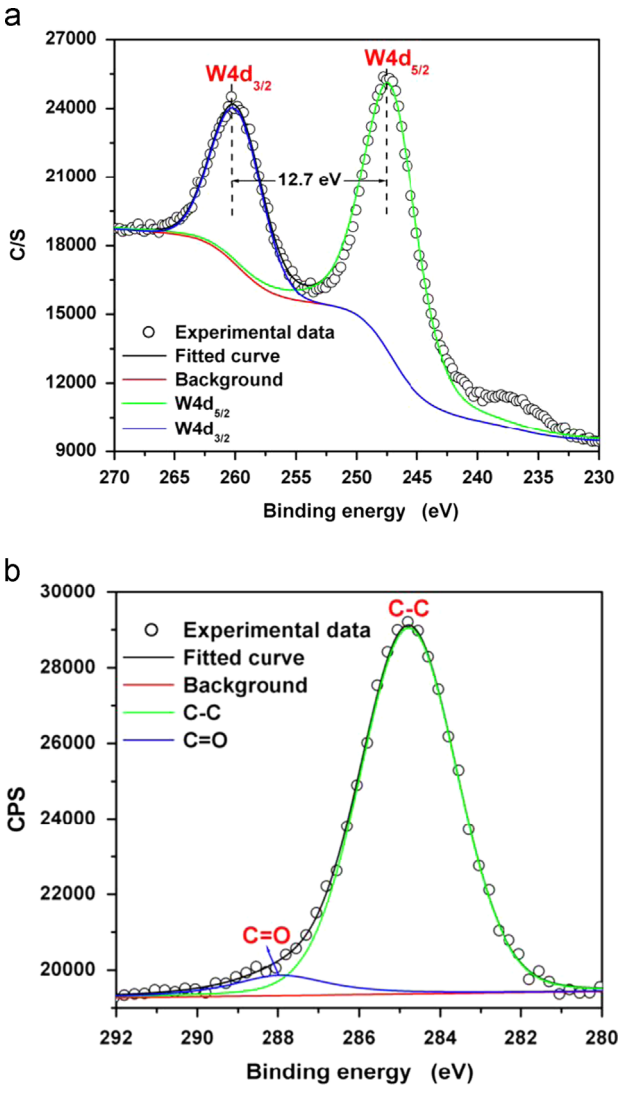

Fig. 3. XPS spectra: (a) W4d peaks and (b) C1s peaks of the GNS-W composite.

characteristics of G, D and 2D bands. In the Raman spectrum, the well-known G band corresponds to the first-order scattering of the E_{2g} mode observed for sp^2-hybridized C–C bonds in a two-dimensional hexagonal lattice, whereas the D band is associated with sp^3-hybridized carbon, defects and disorder carbon in the graphite layers. The broad 2D peak (ca. 2700 cm^{-1}) in the Raman spectrum is the most prominent feature of graphene. The Raman spectrum of the GNS-W composite shown in Fig. 2 clearly displays a broad D band at about 1340 cm^{-1}, a broad G band at 1587 cm^{-1}, and the weak and broadened 2D peak at about 2700 cm^{-1}, indicating a typical features of graphene sheets [20–22]. The intensity ratio of the D band to the G band (I_D/I_G) is usually used to estimate the defect, disorder and average size of the graphitized structure and fraction of sp^3/sp^2-bonded carbon [32]. The intensity ratio of the D- and the G-bands is $I_D/I_G = 1.02$ for GNS-W nanocomposite, indicating a decrease in the size of the in-plane sp^2 domains. Such a result further confirms that the crystalline structure graphene-tungsten oxide composite has been obtained. This result is also consistent with the XRD analysis as mentioned above.

In order to further understand the surface information of the obtained sample, XPS was carried out to analyze the surface/near surface chemical compositions of the GNS-W material. It can be clearly seen that XPS survey spectra confirmed the high chemical purity of the GNS-W composite, consisting solely of W, O and C. Spectra of individual line of W4d measured at high resolution show (Fig. 3(a)) narrow range scans for GNS-W composite. The XPS spectra show two peaks of $4d_{5/2}$ and $4d_{3/2}$ at 247.5 and 260.2 eV with a better symmetry, respectively, and they are assigned to the lattice tungsten in tungsten oxide. They have a peak separation of 12.7 eV between these two peaks. The values correspond to a binding energy of W(VI) ion (indexed Standard ESCA Spectra of the Elements and Line Energy Information, Co., USA). The C1s peak (Fig. 3(b)) of graphene in GNS-W could be deconvoluted into two components at binding energies of 284.8 eV (C–C) and 287.9 eV (C═O), which indicates that there are still some residual oxygen-containing functionalities on the reduced graphene sheets because of incomplete reduction.

The microstructure and morphology of the GNS-W composite were studied by scanning electron microscopy (SEM). Fig. 4(a) and (b) show the SEM images of the GNS-W composite, in which the graphene nanosheets appear a wavy shape. GNS and tungsten oxide recombine to form composite and exhibit a packed layer structure. The morphology of the GNS-W composite was further observed by transmission electron microscopy (TEM). Fig. 4(c) and (d) clearly show that the GNS appears as a transparent thin film and is decorated with a dispersion of WO_3–$WO_3 \cdot H_2O$ mixtures platelets with lengths and widths of 50–150 nm. Furthermore, the tungsten oxides were anchored on the surface of the GNS

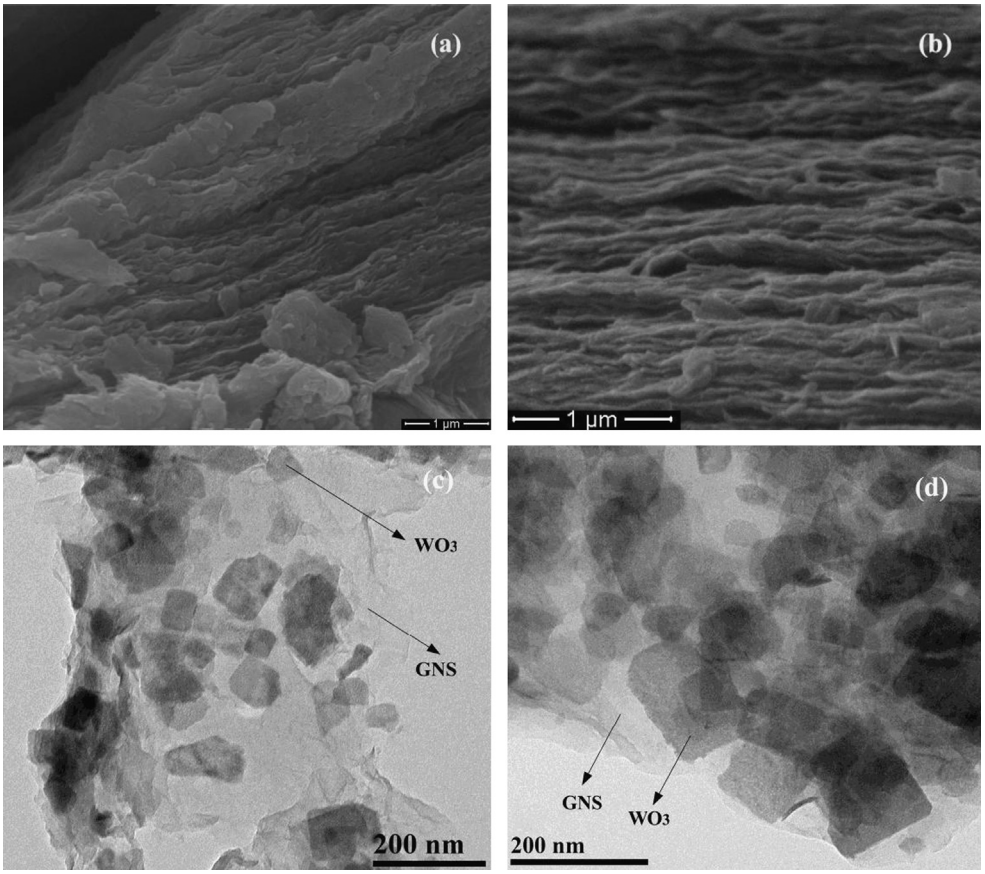

Fig. 4. (a and b) SEM and (c and d) TEM images of the GNS-W composite.

acted as spacers, which prevented the restacking of graphene sheets, thereby increasing the active surface for electrochemical reactions.

Fig. 5(a) shows CV curves of GNS-W composite electrode under the potential from 0.0 to 1.0 V and the different scan rates. The characteristics of the peaks of supercapacitors are clearly observed. The CV loops in our experiment are no-rectangular and gradually distorted with an increment of sweep rate due to the internal resistance of the composite electrode. As can be seen from Fig. 5(a), all the CV loops without obvious redox peaks indicate that the electrode has a good capacitive behavior. The galvanostatic charge–discharge curves of the GNS-W composite electrode in a 1 M H_2SO_4 electrolyte are shown in Fig. 5(b), which were measured at different current densities from 0.1 to 1.0 A g^{-1}. It is evident that a characteristic pseudocapacitive behavior is observed for GNS-W composite electrode. The potential responses of the GNS-W composite during charge and discharge are nearly symmetrical. Although the shape of the charge–discharge curves did not show a typical triangular shape, a similar trend was observed for other tungsten oxide materials in 1 M H_2SO_4 electrolyte [33]. For comparison, the $WO_3/WO_3 \cdot H_2O$ mixtures electrode was also tested under the same electrochemical conditions. Fig. 5(c) shows the CV curves of the GNS-W composite and the tungsten oxides electrode under the scan rate of 30 mV s^{-1}, respectively. It is striking to note that the maximal integral area of the CV loop for the GNS-W electrode is even larger than that for the tungsten oxides electrode, which indicates the composite produces positive synergistic effects in specific capacitance. The galvanostatic charge/discharge was also conducted to obtain the specific capacitance of GNS-W composite. According to the galvanostatic discharge curves, the specific capacitance of all the electrodes is calculated using the following formula:

$$C = \frac{I\Delta t}{m\Delta V}$$

where C is specific capacitance (F g^{-1}), I is discharge current (A), m is the mass of active material (g),Δt is the total discharge time, and ΔV is the potential drop during discharging. Fig. 5(d) displays the typical discharge/charge profiles of the GNS-W composite and the tungsten oxides at current density of 0.3 A g^{-1} between the voltage limits of 0–1.0 V. The specific capacitances of the GNS-W composite and the tungsten oxides are calculated to be 140.8 and 24.5 F g^{-1}, respectively.

Fig. 6(a) compares the rate capabilities of the GNS-W composite and the tungsten oxides at different rates. The discharge

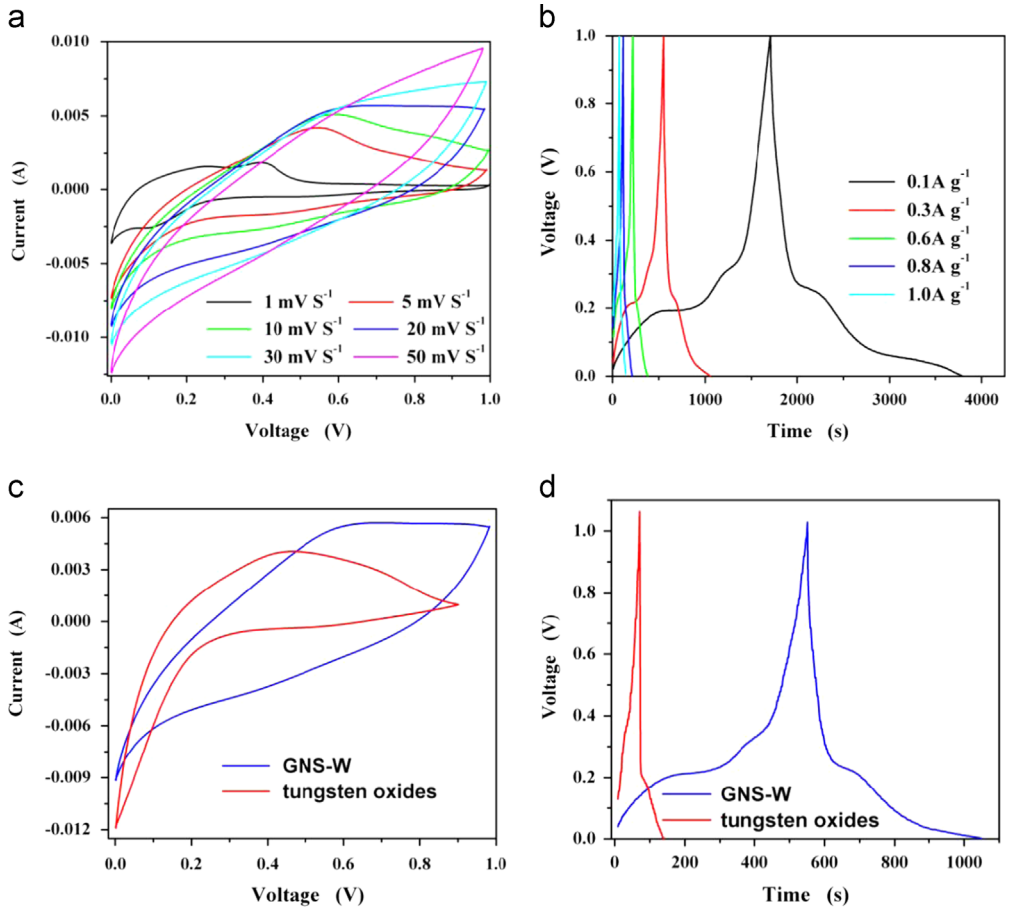

Fig. 5. (a and b) CV and galvanostatic charge–discharge curves of the GNS-W composite electrode at different scan rates and current densities in a 1 M H_2SO_4 electrolyte, respectively. (c) CV curves of the tungsten oxides and the GNS-W composite at a scan rate of 20 mV s^{-1}. (d) Galvanostatic charge–discharge curves of the tungsten oxides and the GNS-W composite at a current density of 0.3 A g^{-1}.

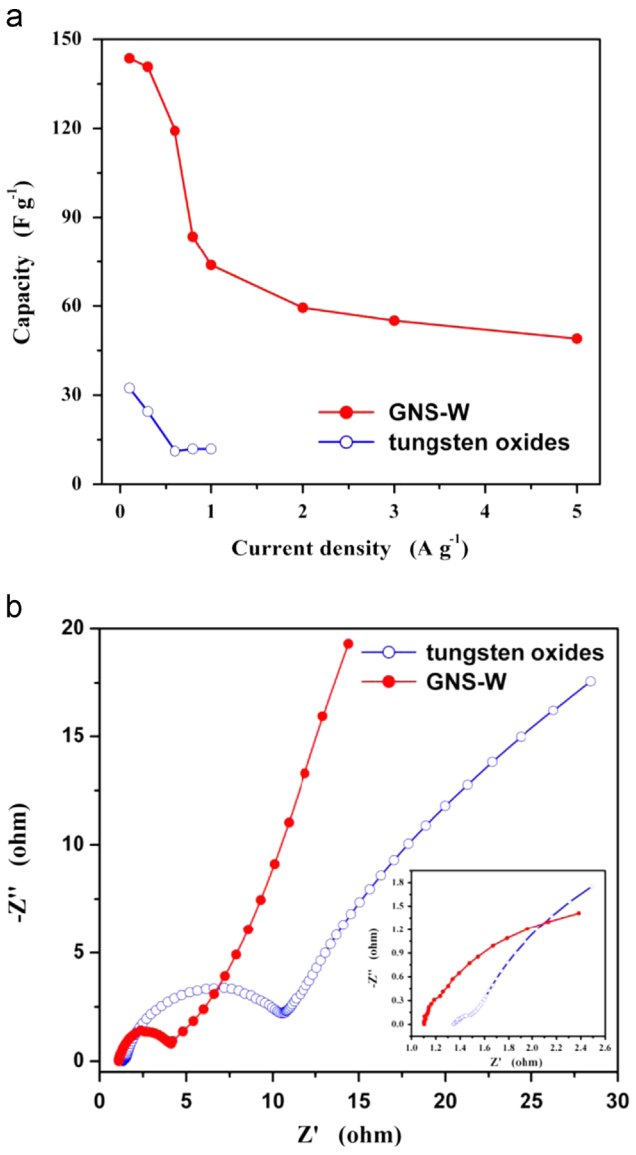

Fig. 6. (a) Comparison of the rate capabilities of the tungsten oxides and the GNS-W electrodes at different rates, (b) EIS curves of the tungsten oxides and the GNS-W composite.

specific capacitance of all electrodes decreases steeply with increasing discharge rate. The GNS-W composite electrode has a specific capacitance of 143.6 F g^{-1} at a low current density of 0.1 A g^{-1}, which increases 343 % compared with that of the pure WO_3 (32.4 F g^{-1}). This value is also higher compared with some reported results of the tungsten oxides [7,10,12,34], which is attributed to the capacitance contributed from the participation of GNS and the composition of GNS resulting in the lower charge transfer resistance. As shown, the specific capacitance of GNS-W composite electrode gradually decreases with charge–discharge current density increasing, and the value reduces to 48.9 F g^{-1} (34% capacitance of 0.1 A g^{-1}) at a high current density of 5 A g^{-1}. This may be due to the sluggish redox reaction kinetics and low penetration of sulfate ions in and out of the electrode at fast potential changes [35]. Generally, the electrochemical impedance spectroscopy (EIS) is an important parameter to examine the performances of supercapacitors. The impact of GNS addition on the electrical conductivity of the GNS-W composite electrode could be investigated using EIS studies. Fig. 6(b) presents the Nyquist plots of synthesized GNS-W composite and $WO_3/WO_3 \cdot H_2O$ mixtures. A semi-circle arc in the high-frequency region and an inclined line in the low frequency region have been observed for GNS-W composite electrode. In generally, the diameter of the semicircle gives the associated charge-transfer resistance and the inclined line is attributable to Warburg impedance, which results from the frequency dependence of ion diffusion and transport in the electrolyte [36]. From Fig. 6(b), it can be seen that the GNS-W composite electrode exhibits a smaller semicircle than the tungsten oxides electrode, which indicates that the GNS-W composite electrode has a lower resistance and a more linear vertical curve than the tungsten oxides electrode. The charge-transfer resistance can be directly measured as the semicirclearc diameter [37]. The value of charge-transfer resistance for GNS-W composite electrode is 4.14 Ω, whereas a much higher charge-transfer resistance of 10.56 Ω was obtained for the tungsten oxides electrode, indicating that the incorporation of GNS improves the charge transfer performance of the GNS-W composite electrode. At the lower frequencies, a straight sloping line represents the diffusive resistance (Warburg impendence, W) of the electrolyte in electrode pores and the proton diffusion in host materials [38]. The diffusing lines for GNS-W composite electrode shows a more linear vertical curve, indicating that the materials have lower diffusion resistance than that of the tungsten oxides electrode. This result is probably due to the fact that the graphene sheets form a conductive network, which facilitates the fast electron transfer between the active materials and the charge collector. It demonstrates that the addition of graphene nanosheets enhances the conductivity of composites. The above feature is of great significance for the electrochemical behavior of a supercapacitor.

The good electrochemical properties of the GNS-W composite material could result from the interaction between the tungsten oxides platelets and the edges of GNS. On the one hand, when tungsten oxides were deposited on the edges and planes of the GNS, they entered into the graphene plane as spacers, which efficiently prevent any serious stacking of the GNS and thus increases the active sites for the electrochemical reaction. Furthermore, the electrolyte active spices easily access the surface of the GNS, which facilitates the formation of electric double layers and improve the utilization of tungsten oxides during the electrochemical process. The similar conclusions can be found in GNS-Fe_3O_4 [39] and GNS-Sn composite electrodes [40]. On the other hand, the addition of GNS could reduce the intrinsic resistance of $WO_3/WO_3 \cdot H_2O$ mixtures due to the graphene sheets conductive network. Therefore, the electrochemical properties of GNS-W composite are corresponding improved. As a result, the GNS-W composite material possesses a good electrochemical performance, which provides an important electrode material candidate for supercapacitors.

4. Conclusions

The GNS-W composite was successfully synthesized using a facile precipitation method. The morphology and the structural characterization of the GNS-W composite were investigated. The prepared composite material consists of tungsten oxides (50–150 nm in size) distributed on separated graphene nanosheets. The electrochemical capacitive behavior of the GNS-W composite and the $WO_3/WO_3 \cdot H_2O$ mixtures has been demonstrated in 1 M H_2SO_4 electrolyte between 0 and 1.0 V. In comparison with the specific capacitance of pure WO_3 electrode, GNS-W composite electrode shows a high specific capacitance of about 143.6 F g^{-1} at a current density of 0.1 A g^{-1}, which is significantly improved. The good electrochemical capacitive derived from GNS-W composite demonstrates a strong synergistic effect due to the improved conductivity of the $WO_3/WO_3 \cdot H_2O$ mixtures and better ion diffusion rate between the tungsten oxides and the edges of GNS.

Acknowledgments

This work was supported by the Department of Science and Technology of Yunnan Province via the Key Project for the Science and Technology (Grant no. 2011FA001), the National Natural Science Foundation of China (Grant no. 51262029), and the State Key Laboratory of Silicon Materials visiting scholar Fund (Grant no. SKL2012-16).

References

[1] X.L. Li, T.J. Lou, X.M. Sun, Y.D. Li, Highly sensitive WO_3 hollow-sphere gas sensors, Inorganic Chemistry 43 (2004) 5442–5449.
[2] T. He, Y. Ma, Y. Cao, X.L. Hu, H.M. Liu, G.J. Zhang, W.S. Yang, J. N. Yao, Photochromism of WO_3 colloids combined with TiO_2 nanoparticles, Journal of Physical Chemistry B 106 (2002) 12670–12676.
[3] M. Hibino, W. Han, T. Kudo, Electrochemical lithium intercalation into a hexagonal WO_3 framework and its structural change, Solid State Ionics 135 (2000) 61–69.
[4] B. Zhang, J.D. Liu, S.K. Guan, Y.Z. Wan, Y.Z. Zhang, R.F. Chen, Synthesis of single-crystalline potassium-doped tungsten oxide nanosheets as high-sensitive gas sensors, Journal of Alloys and Compounds 439 (2007) 55–58.
[5] Q. Xiang, G.F. Meng, H.B. Zhao, Y. Zhang, H. Li, W.J. Ma, J.Q. Xu, Au nanoparticle modified WO_3 nanorods with their enhanced properties for photocatalysis and gas sensing, Journal of Physical Chemistry C 114 (2010) 2049–2055.
[6] S.Y. Liu, F. Zhang, H. Li, T. Chen, Y.D. Wang, Acetone detection properties of single crystalline tungsten oxide plates synthesized by hydrothermal method using cetyltrimethyl ammonium bromide supermolecular template, Sensors and Actuators B: Chemical 162 (2012) 259–268.
[7] C.C. Huang, W. Xing, S.P. Zhuo, Capacitive performances of amorphous tungsten oxide prepared by microwave irradiation, Scripta Materialia 61 (2009) 985–987.
[8] H. Farsi, F. Gobal, Z. Barzgari, A study of hydrated nanostructured tungsten trioxide as an electroactive material for pseudocapacitors, Ionics 19 (2013) 287–294.
[9] S.H. Yoon, E. Kang, J.K. Kim, C.W. Lee, J. Lee, Development of high-performance supercapacitor electrodes using novel ordered mesoporous tungsten oxide materials with high electrical conductivity, Chemical Communications 47 (2011) 1021–1023.
[10] O. Kartachova, A.M. Glushenkov, Y.H. Chen, H.Z. Zhang, X.J. Dai, Y. Chen, Electrochemical capacitance of mesoporous tungsten oxynitride in aqueous electrolytes, Journal of Power Sources 220 (2012) 298–305.
[11] C. Jo, I. Hwang, J. Lee, C.W. Lee, S. Yoon, Investigation of pseudocapacitive charge-storage behavior in highly conductive ordered mesoporous tungsten oxide electrodes, Journal of Physical Chemistry C 115 (2011) 11880–11886.
[12] K.H. Chang, C.C. Hu, C.M. Huang, Y.L. Liu, C.I. Chang, Microwave-assisted hydrothermal synthesis of crystalline WO_3–$WO_3 \cdot 0.5H_2O$ mixtures for pseudocapacitors of the asymmetric type, Journal of Power Sources 196 (2011) 2387–2392.
[13] R. Kötz, M. Carlen, Principles and applications of electrochemical capacitors, Electrochimica Acta 45 (2000) 2483–2498.
[14] E. Kang, S. An, S. Yoon, J.K. Kim, J. Lee, Ordered mesoporous WO_{3-X} possessing electronically conductive framework comparable to carbon framework toward long-term stable cathode supports for fuel cells, Journal of Materials Chemistry 20 (2010) 7416–7421.
[15] J.W. Qin, M.H. Cao, C.W. Hu, Graphene-wrapped WO_3 nanoparticles with improved performances in electrical conductivity and gas sensing properties, Journal of Materials Chemistry 21 (2011) 17167–17174.
[16] Y.L. Chen, Z.A. Hu, Y.Q. Chang, H.W. Wang, Z.Y. Zhang, Y.Y. Yang, H.Y. Wu, Zinc oxide/reduced graphene oxide composites and electrochemical capacitance enhanced by homogeneous incorporation of reduced graphene oxide sheets in zinc oxide matrix, Journal of Physical Chemistry C 115 (2011) 2563–2571.
[17] C.C. Xiang, M. Li, M.J. Zhi, A. Manivannan, N.Q. Wu, Reduced graphene oxide/titanium dioxide composites for supercapacitor electrodes: shape and coupling effects, Journal of Materials Chemistry 22 (2012) 19161–19167.
[18] S.M. Paek, E. Yoo, I. Honma, Enhanced cyclic performance and lithium storage capacity of SnO_2/graphene nanoporous electrodes with three-dimensionally delaminated flexible structure, Nano Letters 9 (2009) 72–75.
[19] Z.P. Li, Y.J. Mi, X.H. Liu, S. Liu, S.R. Yang, J.Q. Wang, Flexible graphene/MnO_2 composite papers for supercapacitor electrodes, Journal of Materials Chemistry 21 (2011) 14706–14711.
[20] Y. Wang, C.X. Guo, J.H. Liu, T. Chen, H.H. Yang, C.M. Li, CeO_2 nanoparticles deposited on three-dimensional graphene as supercapacitors with high power density, Dalton Transactions 40 (2011) 6388–6391.
[21] B. Wang, Y. Wang, J. Park, H. Ahn, G.X. Wang, In situ synthesis of Co_3O_4/graphene nanocomposite material for lithium-ion batteries and supercapacitors with high capacity and supercapacitance, Journal of Alloys and Compounds 509 (2011) 7778–7783.
[22] B. Zhao, J.S. Song, P. Liu, W.W. Xu, T. Fang, Z. Jiao, H.J. Zhang, Y. Jiang, Monolayer graphene/NiO nanosheets with two-dimension structure for supercapacitors, Journal of Materials Chemistry 21 (2011) 18792–18798.
[23] Z.S. Wu, G.M. Zhou, L.C. Yin, W.C. Ren, F. Li, H.M. Cheng, Graphene/metal oxide composite electrode materials for energy storage, Nano Energy 1 (2012) 107–131.
[24] F.H. Li, J. Song, H. Yang, S. Gan, Q. Zhang, D. Han, A. Ivaska, One-step synthesis of graphene/SnO_2 nanocomposites and its application in electrochemical supercapacitors, Nanotechnology 20 (2009) 455602.
[25] M. Law, L.E. Greene, J.C. Johnson, R. Saykally, P.D. Yang, Nanowire dye-sensitized solar cells, Nature Materials 4 (2005) 455–459.
[26] C. Zhu, S. Guo, Y. Fang, S. Dong, Reducing sugar: new functional molecules for the green synthesis of graphene nanosheets, ACS Nano 4 (2010) 2429–2437.
[27] J. Wang, Z. Gao, Z.S. Li, B. Wang, Y.X. Yan, Q. Liu, T. Mann, M. L. Zhang, Z.H. Jiang, Green synthesis of graphene nanosheets/ZnO composites and electrochemical properties, Journal of Solid State Chemistry 184 (2011) 1421–1427.
[28] S. Rajagopal, D. Nataraj, D. Mangalaraj, Y. Djaoued, J. Robichaud, O. Yu. Khyzhun, Controlled growth of WO_3 nanostructures with three different morphologies and their structural, optical, and photodecomposition studies, Nanoscale Research Letters 4 (2009) 1335–1342.
[29] I.M. Szilágyi, J. Madarász, G. Pokol, P. Király, G. Tárkányi, S. Saukko, J. Mizsei, A.L. Tóth, A. Szabó, K. Varga-Josepovits, Stability and

controlled composition of hexagonal WO_3, Chemistry of Materials 20 (2008) 4116–4125.
[30] C. Santato, M. Odziemkowski, M. Ulmann, J. Augustynski, Crystallographically oriented mesoporous WO_3 films: synthesis, characterization, and applications, Journal of the American Chemical Society 123 (2001) 10639–10649.
[31] O. Yayapaoa, T. Thongtema, A. Phuruangratb, S. Thongtem, CTAB-assisted hydrothermal synthesis of tungsten oxide microflowers, Journal of Alloys and Compound 509 (2011) 2294–2299.
[32] V. Chandra, J. Park, Y. Chun, J.W. Lee, I.C. Hwang, K.S. Kim, Water-dispersible magnetite-reduced graphene oxide composites for arsenic removal, ACS Nano 4 (2010) 3979–3986.
[33] R. Ganesan, I. Perelshtein, A. Gedanken, Singlet oxygen chemistry in water: a porous vycor glass-supported photosensitizer, Journal of Physical Chemistry C 112 (2008) 1913–1917.
[34] B.X. Zoua, Y. Liang, X.X. Liu, D. Diamond, K.T. Lau, Electrodeposition and pseudocapacitive properties of tungsten oxide/polyaniline composite, Journal of Power Sources 196 (2011) 4842–4848.
[35] Z. Fan, J. Yan, T. Wei, L. Zhi, G. Ning, T. Li, F. Wei, Asymmetric supercapacitors based on graphene/MnO_2 and activated carbon nanofiber electrodes with high power and energy density, Advanced Functional Materials 21 (2011) 2366–2375.
[36] Y.J. Guo, S.J. Guo, J.T. Ren, Y.M. Zhai, S.J. Dong, E. Wang, Graphene hybrid nanosheets with high supramolecular recognition capability: synthesis and host-guest inclusion for enhanced electrochemical performance, ACS Nano 4 (2010) 4001–4010.
[37] H.L. Guo, X.F. Wang, Q.Y. Qian, F.B. Wang, A green approach to the synthesis of graphene nanosheets, ACS Nano 3 (2009) 2653–2659.
[38] W. Sugimoto, H. Iwata, K. Yokoshima, Y. Murakami, Y. Takasu, Proton and electron conductivity in hydrous ruthenium oxides evaluated by electrochemical impedance spectroscopy: the origin of large capacitance, Journal of Physical Chemistry B 109 (2005) 7330–7338.
[39] K. Karthikeyan, D. Kalpana, S. Amaresh, Y.S. Lee, Microwave synthesis of graphene/magnetite composite electrode material for symmetric supercapacitor with superior rate performance, RSC Advances 2 (2012) 12322–12328.
[40] Z. Qin, Z.J. Li, M. Zhang, B.C. Yang, R.A. Outlaw, Sn nanoparticles grown on graphene for enhanced electrochemical properties, Journal of Power Sources 217 (2012) 303–308.